

Classification of autoimmune diseases from Peripheral blood TCR repertoires by multimodal multi-instance learning

Ruihao Zhang^{1,*}, Fei Ye², Dandan Meng², Yixuan Huang³, Maochen⁴, Xiao Liu^{*}

Tsinghua Shenzhen International Graduate School

Tsinghua University

Shenzhen, China

* Corresponding authors: zhangrh23@mails.tsinghua.edu.cn, liuxiao@sz.tsinghua.edu.cn

Abstract—T cell receptor (TCR) repertoires encode critical immunological signatures for autoimmune diseases, yet their clinical application remains limited by sequence sparsity and low witness rates. We developed EAMil, a multi-instance deep learning framework that leverages TCR sequencing data to diagnose systemic lupus erythematosus (SLE) and rheumatoid arthritis (RA) with exceptional accuracy. By integrating PrimeSeq feature extraction with ESMonehot encoding and enhanced gate attention mechanisms, our model achieved state-of-the-art performance with AUCs of 98.95% for SLE and 97.76% for RA. EAMil successfully identified disease-associated genes with over 90% concordance with established differential analyses and effectively distinguished disease-specific TCR genes. The model demonstrated robustness in classifying multiple disease categories, utilizing the SLEDAI score to stratify SLE patients by disease severity as well as to diagnose the site of damage in SLE patients, and effectively controlling for confounding factors such as age and gender. This interpretable framework for immune receptor analysis provides new insights for autoimmune disease detection and classification with broad potential clinical applications across immune-mediated conditions.

Keywords—autoimmune diseases, PrimeSeq, ESMonehot, enhanced gate attention, EAMIL

I. INTRODUCTION

Autoimmune diseases arise from fundamental dysregulation of immune tolerance, where the body's defense system incorrectly recognizes self-tissues as foreign, triggering inappropriate antibody production and cellular immune responses against endogenous components [1]. The global prevalence of these conditions has increased markedly, particularly in industrialized nations, creating significant public health challenges [2,3]. Systemic lupus erythematosus (SLE) exemplifies this disease category, characterized by multisystem involvement affecting skin, joints, kidneys, and the central nervous system, often leading to severe organ dysfunction [4,5]. Rheumatoid arthritis (RA) represents another major autoimmune disorder, distinguished by its complex cytokine-mediated pathophysiology and chronic inflammatory joint destruction, frequently accompanied by systemic manifestations [6,7]. Current diagnostic approaches rely on comprehensive clinical assessment integrating patient history, radiological findings, and autoantibody testing—a process that is typically protracted and complex [8,9].

T cells have emerged as central players in autoimmune pathogenesis. Autoreactive T cell populations, observed in both peripheral circulation and affected tissues of SLE and RA patients, strongly implicate these cells in disease development and progression. The T cell receptor (TCR) serves as the critical molecular interface for antigen recognition, with the TCR beta chain (TRB) representing one of its most diverse and informative components. TRB diversity derives from combinatorial rearrangement of variable (V), diversity (D), and joining (J) gene segments, with the region spanning the V-segment terminus to the J-segment beginning encoding the complementarity-determining region 3 (CDR3) [10]. High-throughput sequencing technologies have revealed significant alterations in V-gene selection, V-J pairing patterns, and CDR3 composition in autoimmune populations compared to healthy controls [11]. Moreover, TCR diversity metrics and clonal dynamics correlate with disease status and progression, offering potential biomarkers for diagnosis, monitoring, and prognosis [11,12,13]. Consequently, comprehensive TCR repertoire analysis promises to illuminate autoimmune pathogenesis while potentially revolutionizing precision medicine approaches.

The convergence of high-throughput TCR sequencing technologies and advanced computational methods has created unprecedented opportunities for autoimmune disease prediction through deep learning frameworks. However, significant challenges persist in this nascent field. First, the extraordinary diversity and similarity within TCR repertoires complicates the identification of disease-specific sequence features. Autoimmune pathogenesis typically involves aberrant expression of relatively few specific TCR sequences against a vast background of disease-irrelevant sequences, resulting in an exceptionally low witness rate (WR) [14]. Second, the massive scale of TCR sequencing data imposes substantial computational demands, necessitating models that balance analytical power with processing efficiency [15]. Third, current approaches often assign sample-level labels directly to sequences, hindering the identification of disease-associated TCRs and limiting model interpretability [16]. Finally, the weak labeling paradigm—where repertoires are annotated only with patient disease status rather than sequence-specific disease associations—restricts traditional classification approaches and demands more sophisticated multi-instance learning methodologies [11].

Previous computational approaches have demonstrated variable success in addressing these challenges. Maxim E et al. employed ensemble learning to integrate BCR and TCR data for immunological diagnosis, though performance on TCR data alone remained suboptimal [17]. John-William demonstrated deep learning's potential for improved TCR featurization across multiple datasets, enhancing antigen-specific TCR classification, yet employed relatively coarse sequence handling and weak label management [16]. Tongfei et al. combined CNN and Bi-LSTM architectures for autoimmune disease diagnosis, but their dictionary mapping approach struggled with large-scale CDR3 sequence analysis, and model interpretability remained limited [18]. The field continues to lack deep learning frameworks that efficiently extract disease-relevant sequences and gene features from weakly-labeled TCR repertoires while maintaining interpretability.

The emergence of Transformer architectures and large language models (LLMs) has revolutionized bioinformatics, particularly for protein sequence modeling [19]. Pretrained models like ESM2, developed on extensive protein datasets, capture complex sequence relationships and demonstrate robust cross-domain generalization capabilities [20]. We leverage these advances by implementing ESM2 for extracting and encoding CDR3 amino acid sequence information, complemented by one-hot encoding for V-gene representation. Our integrated ESMonehot module thus capitalizes on both ESM2's protein representation capabilities and V-gene information to comprehensively characterize TCR features.

Fundamentally, autoimmune disease prediction from TCR repertoires represents a multimodal multi-instance learning (MIL) challenge, where each sequencing sample constitutes a "bag" containing multiple TCR sequence "instances" [21]. Since individual health status typically correlates with variations in only a subset of specific TCR sequences, and instance-level labels are generally unavailable, this scenario aligns perfectly with weakly-supervised MIL paradigms. While MIL has demonstrated remarkable success in domains like pathological image analysis [22,23,24], its application to TCR-based autoimmune disease prediction remains underexplored. We therefore propose transferring established MIL architectures and algorithms from image analysis to sequence domains, addressing the unique challenges of TCR data while expanding MIL's bioinformatic applications.

To this end, we introduce EAMIL, a multimodal multi-instance learning framework integrating the ESMonehot module to extract discriminative features from SLE and RA-associated TCR sequences for disease classification. Our approach implements the PrimeSeq strategy to select high-frequency sequence subsets from expansive TCR datasets, ensuring effective coverage while enabling lightweight processing to overcome low witness rates and computational constraints. EAMIL's multimodal fusion module synthesizes V-gene and amino acid sequence information to generate comprehensive representations that capture disease-state-specific features. The model's attention mechanism effectively identifies and prioritizes disease-associated genes and sequences, enhancing both diagnostic utility and interpretability. Simultaneously, the instance-level MIL mechanism optimizes loss functions across both sample and sequence dimensions, effectively leveraging weak labels.

We comprehensively evaluated EAMIL using TCR sequencing data from SLE, RA, and healthy individuals, conducting binary classification, multi-class classification, and one-versus-others experiments. Comparative analyses against DeepTCR and DeepTAPE demonstrated EAMIL's state-of-the-art performance [16,18]. Beyond classification accuracy, we assessed the model's ability to differentiate between SLE populations with varying Disease Activity Index (SLEDAI) scores and healthy controls [25], while also examining the limited impact of age and gender covariates on diagnostic performance. Our key contributions include:

- Development of EAMIL, a framework that minimizes classification loss through instance-level MIL while ensuring computational efficiency via PrimeSeq and ESMonehot modules, effectively addressing TCR repertoire scale and witness rate challenges;
- Enhanced attention mechanisms are introduced to learn key features holistically and locally, including gating and spatial attention modules to improve the identification of disease-associated genes and sequences. These mechanisms enable effective sequence-level and sample-level training, even with limited sample-level labeling, thereby boosting overall model performance;
- Comprehensive performance evaluation in SLE and RA classification, SLEDAI score stratification, and identification of disease-damage regions in SLE, highlighting EAMIL's potential for clinical diagnostics.

II. METHODS AND MATERIALS

A. Datasets

This study utilized comprehensive TCR sequencing data previously generated through high-throughput sequencing technology [11]. The dataset encompasses peripheral blood samples from 1,522 individuals, meticulously characterized through TCR rearrangement amplification and deep sequencing. The cohort comprises 877 individuals with systemic lupus erythematosus (SLE), 206 with rheumatoid arthritis (RA), and 439 healthy controls. These samples were employed in both binary classification tasks (SLE versus Control, RA versus Control) and multiclass classification analyses integrating all three phenotypes.

Analysis of sequence distribution revealed that most samples contained approximately 10^6 unique CDR3 sequences, presenting significant challenges for feature learning and computational efficiency, as shown in Figure 1a. Implementation of the PrimeSeq strategy substantially reduced dimensionality while preserving critical immunological information. Venn diagram analysis of CDR3 sequences across diagnostic categories demonstrated considerable sequence overlap between phenotypes, highlighting the complexity of classification, as shown in Figure 1b. Notably, CDR3 length distribution exhibited disease-specific patterns, with SLE-derived sequences tending toward longer fragments and RA-associated sequences skewing shorter, providing potentially discriminative features for diagnostic modeling. Within the SLE cohort, patients in active versus quiescent disease states showed similar sequence repertoires but differed significantly in length distribution and frequency patterns, offering a foundation for disease activity stratification, as shown in Figure 1e.

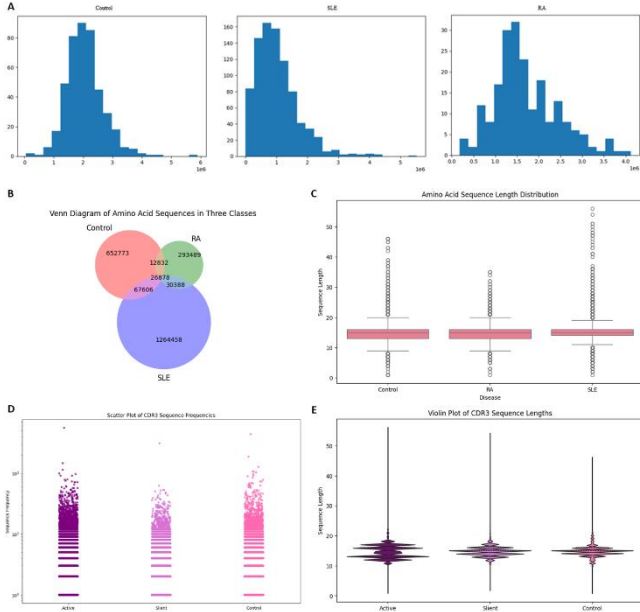


Fig. 1. Distribution of CDR3 sequences. We plotted bar graphs of the distribution of raw CDR3 sequences under the three datasets (A) and plots of the distribution of CDR3 sequence lengths in the three populations after sampling Wayne (B). We plotted the distribution of CDR3 sequence lengths in the three populations after sampling (C). We plotted violin plots of CDR3 sequence length distribution and scatter plots of CDR3 sequence frequency distribution for Active and Silent SLE patients as well as healthy individuals (D, E).

B. Hyperparameters

All experiments were conducted on an NVIDIA RTX4090 GPU to ensure computational reproducibility and experimental consistency. Data processing was implemented using the ESMonehot methodology. This approach integrates one-hot encoding for gene representation (generating 1000-dimensional vectors) with ESM2-derived protein embeddings for amino acid sequences (producing 640-dimensional vectors), culminating in 1640-dimensional feature vectors through concatenation. This multimodal encoding strategy enables comprehensive characterization of diverse TCR features. Model optimization employed the Adam optimizer with carefully calibrated hyperparameters: a learning rate of 0.0002 for transfer learning applications and a weight decay coefficient of 0.00001, balancing learning capacity with generalization potential. To ensure experimental reproducibility, we fixed the random seed at 2024. Model overfitting was prevented through strategic implementation of dropout (ratio 0.1), providing effective regularization to enhance generalization performance on unseen data.

C. Problem Definition

The autoimmune disease prediction task was formulated within a multiple instance learning (MIL) framework. The experimental dataset comprises N independent samples, denoted as $\{S_1, S_2, \dots, S_n\}$, where each sample S_i contains M_i sequences represented as $\{S_i^1, S_i^2, \dots, S_i^{M_i}\}$. Notably, sequence count M_i varies between samples. Each sample S_i corresponds to a diagnostic label L_i , collectively forming the label set $\{L_1, L_2, \dots, L_n\}$, where L takes values in $\{0, \dots, C\}$, with C representing the total class count. For binary classification between autoimmune disease and healthy populations, $C = 2$.

The objective is to construct a prediction function F such that for any test sample S , the function $Y = F(S)$ accurately predicts its corresponding disease state L . We implemented a strategy utilizing sample-level labels L_i as pseudo-labels for the corresponding TCR repertoire $\{S_i^1, S_i^2, \dots, S_i^{M_i}\}$. This approach enables the model to learn effective feature extraction from sequence collections during training, ultimately achieving robust sample-state prediction.

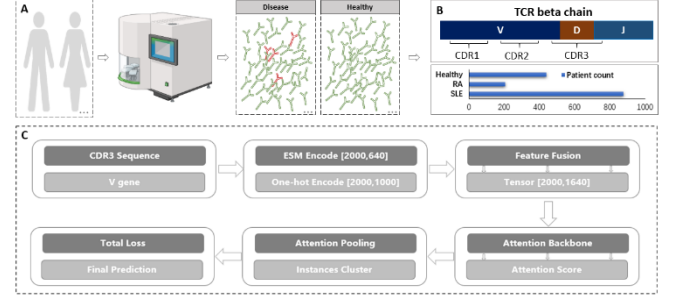


Fig. 2. Data processing pipeline of the EAMIL model. We use 1552 samples obtained from high-throughput sequencing. The model mainly consists of feature selection and encoding, attention mechanism, attention pooling, and instance level clustering to finally obtain the prediction results.

D. Data Processing Pipeline

Following selection of CDR3 sequences and relevant genes, our model independently encodes these features. Each feature within a sample is transformed into a $[2000, 640]$ -dimensional tensor by the pretrained ESM protein language model. These multi-feature tensors are subsequently concatenated and preserved as encoded files, serving as input for the multi-instance module. The attention mechanism computes corresponding attention scores for each sample. Through Attention Pooling, we derive sample-level classification loss, while the instance clustering methodology generates instance-level clustering loss. These complementary loss functions collaboratively guide model training for precise data analysis and prediction, as shown in Figure 2c.

E. Model Architecture

We introduce EAMIL, a deep learning framework specifically engineered for TCR sequence analysis. Based on data extracted through the PrimeSeq strategy, EAMIL employs ESMonehot feature extraction, utilizing a pretrained ESM encoder for CDR3 sequences and one-hot encoding for TCR gene segments, generating high-dimensional feature vector representations. The model implements multi-instance learning (MIL) with an enhanced gated attention mechanism to identify important features and a clustering strategy that leverages bag-level labels as pseudo-labels to optimize training and enhance classification performance. This approach facilitates feature learning at both sequence and sample levels, as shown in Figure 3. The following sections detail these architectural components.

• Feature Extraction Module

TCR sequencing generates massive datasets with substantial background noise. Extracting the rare but critical disease-associated signals from this extensive data is essential for computational efficiency and effective information mining. PrimeSeq strategy addresses this challenge by incorporating

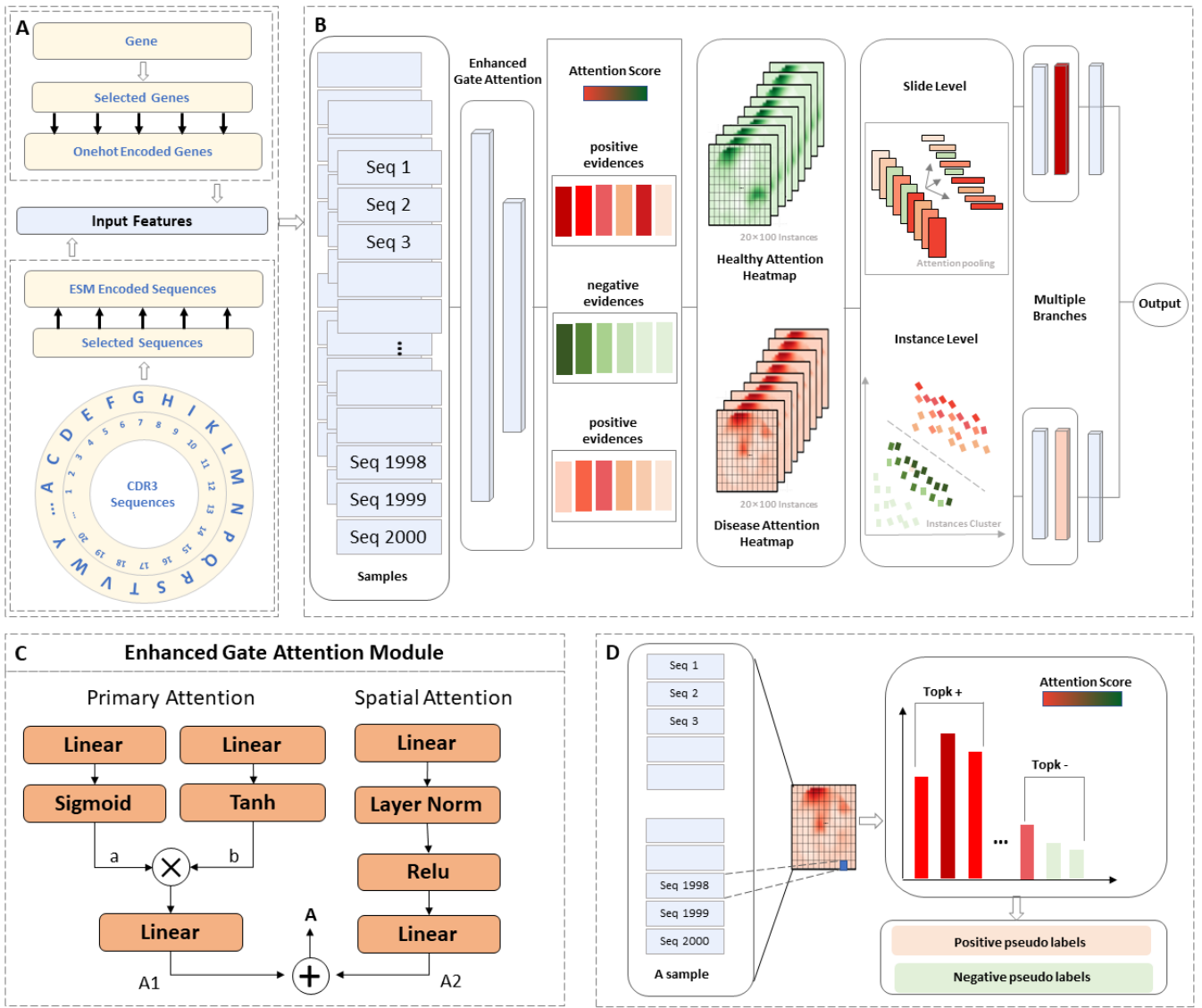


Fig. 3. Framework of EAMIL model. It mainly consists of feature extractor, enhanced gate attention module and multi-instance deep learning module, aiming to achieve deep analysis and understanding of complex bioinformatics data. Based on the key data extracted by PrimeSeq strategy, the EAMIL model employs the ESMonehot feature extraction technique to generate a high-dimensional feature vector representation (A). Then, the model adopts a multi-instance learning (MIL) approach to introduce enhanced gate attention mechanism, followed by a pooling and clustering strategy that utilizes bag-level labels as pseudo-labels to optimize the training process of the model and significantly improve the classification performance, and learns features from both sequence and sample levels (B). Through the gated attention mechanism and spatial attention mechanism, the model can model the input features at multiple levels, both globally and locally, to enhance the flexibility and diversity of the attention mechanism (C). Through the enhanced gate attention mechanism, we can obtain the attention score of each sequence and assign pseudo-labels to the k sequences with the highest attention score (D).

frequency information, selectively extracting high-frequency sequences to ensure representation of characteristic sample features. This targeted extraction significantly reduces encoding requirements, effectively addressing the challenges of low witness rate (WR) and extensive TCR sequence and gene data.

To comprehensively characterize TCR repertoires, we designed a multimodal fusion encoding module integrating CDR3 sequences with gene segment information. For sequences obtained through the PrimeSeq strategy, we applied the ESMonehot module for encoding. Specifically, the pretrained ESM model encodes sampled CDR3 sequences while gene fragments are represented through one-hot encoding, as shown in Figure3a. These encodings are

concatenated along a specific dimension to form a fusion feature matrix, with subsequent pooling to generate sequence-level features. This combination of protein language model pretraining and multimodal fusion produces a synthesized representation matrix that comprehensively captures TCR receptor characteristics, providing enriched information for disease prediction and classification.

- **Enhanced Gate Attention Module**

The Enhanced Gate Attention Module is a dual-pathway attention mechanism designed to optimize feature extraction by integrating global and spatial sensitivity. This module addresses the limitations of conventional attention mechanisms in capturing both global contextual dependencies and localized feature patterns, enabling the extraction of

enriched representations critical for downstream tasks such as classification and disease prediction. By combining a primary gated attention mechanism with an auxiliary spatial attention branch, the module achieves a synergistic feature representation that enhances model performance in complex data environments.

The primary attention branch operates on input features $x \in \mathbb{R}^{n \times L}$, where L is the feature dimensionality, and n represents the number of input samples. This branch applies two parallel transformations, the first one is Non-linear activation using Tanh:

$$a = \tanh(W_a x + b_a), \quad W_a \in \mathbb{R}^{D \times L}, b_a \in \mathbb{R}^D \quad (1)$$

Then, it takes Sigmoid-based gating:

$$b = \sigma(W_b x + b_b), \quad W_b \in \mathbb{R}^{D \times L}, b_b \in \mathbb{R}^D \quad (2)$$

The outputs of these two transformations are multiplied element-wise to generate the gated attention weights:

$$A_1 = W_c \cdot (a \odot b) + b_i, \quad W_c \in \mathbb{R}^{n_{classes} \times D}, b_c \in \mathbb{R}^{n_{classes}} \quad (3)$$

This gated attention mechanism ensures that the module selectively amplifies informative patterns while suppressing noise, capturing global contextual dependencies.

To complement the global attention from the primary branch, the module incorporates a spatial attention branch designed to capture localized feature patterns. This branch applies a series of linear transformations, normalization, and non-linear activation to the input x , defined as:

$$A_2 = W_s^{(2)} \cdot \text{RELU}(\text{LayerNorm}(W_s^{(1)} x + b_s^{(1)})) + b_s^{(2)} \quad (4)$$

Where $W_s^{(1)} \in \mathbb{R}^{(D/2) \times L}$, $W_s^{(2)} \in \mathbb{R}^{n_{classes} \times (D/2)}$, and $b_s^{(1)}, b_s^{(2)}$ are bias terms. The spatial attention branch allows the module to focus on fine-grained details, making it particularly effective in tasks where localized variation is important.

The outputs from the two branches are combined to form the final attention score:

$$A = A_1 + \lambda A_2 \quad (5)$$

where λ is a scaling factor that balances the contributions of global and spatial attention. This fused attention score is subsequently used to refine feature representations for downstream tasks, as shown in Figure 3c.

The Enhanced Gate Attention Module offers significant advantages through its dual-pathway design, which effectively integrates global contextual modeling and localized feature sensitivity. The primary gated attention mechanism selectively amplifies critical patterns while suppressing noise, ensuring robust global feature extraction. Simultaneously, the spatial attention branch captures fine-grained, localized variations, enhancing the module's ability to address spatial or positional dependencies. By combining these two pathways, the module produces a comprehensive and enriched feature representation, balancing global and local information. This fusion not only improves robustness and generalization across diverse datasets but also addresses challenges such as high-dimensionality and background noise. Furthermore, the mathematically principled formulation ensures computational efficiency and stable learning dynamics, making the module well-suited for complex tasks such as classification, disease prediction, and sequence analysis.

- Multi-Instance Learning Module

1) *Instance-Level Representation*: The Multi-Instance Learning (MIL) module is implemented using the CLAM-

MB model, which leverages an Enhanced Attention Network with Gating to aggregate instance-level features into sample-level representations. This approach is particularly suited for binary and multi-class classification tasks where each sample consists of a collection of instances, such as sequences, enabling efficient and interpretable learning from complex, high-dimensional data. The core of the CLAM-MB model lies in its trainable and interpretable attention-pooling mechanism, which aggregates instance-level features based on learned attention scores. This mechanism enhances the model's ability to focus on the most informative instances within a sample, facilitating effective feature representation and improving classification performance.

2) *Attention-Pooling Mechanism*: Each sample $z \in \mathbb{R}^{N \times L}$ is represented as a feature matrix consisting of N feature vectors, where L is the dimensionality of the feature space. These feature vectors are derived from prior encoding steps, and each corresponds to an instance within the sample. The MIL setting assumes that only sample-level labels are available, while individual instance labels remain unknown. The Enhanced Gated Attention Network serves as the backbone of the attention mechanism. For each instance $h_k \in \mathbb{R}^L$, the attention score a_k is computed as:

$$a_k = W_a \cdot (\tanh(V_a h_k^T) \odot \delta(U_a h_k^T)) \quad (6)$$

where $W_a \in \mathbb{R}^{1 \times D}$, $V_a \in \mathbb{R}^{D \times L}$, and $U_a \in \mathbb{R}^{D \times L}$ are trainable weight matrices. The \tanh function introduces non-linearity and models interactions between input features and sigmoid activation serves as a gating mechanism, allowing the network to selectively emphasize relevant features while suppressing noise.

The attention scores are normalized across all instances within a sample using the softmax function:

$$a_k = \frac{\exp(a_k)}{\sum_{i=1}^N \exp(a_i)} \quad (7)$$

where a_k represents the normalized attention weight for instance k .

3) *Sample-Level Representation*: The instance-level features are aggregated into a sample-level representation $M \in \mathbb{R}^L$ using the attention weights:

$$M = \sum_{k=1}^N a_k h_k \quad (8)$$

This weighted aggregation ensures that the most informative instances contribute more significantly to the final sample representation, improving the model's ability to classify complex and noisy data.

4) *Classification Heads*: The aggregated feature representation M is passed through a disease classifier for main task classification:

$$\hat{y} = \text{soft max}(W_c M + b_c) \quad (9)$$

Where $W_c \in \mathbb{R}^{n_{classes} \times L}$ and $b_c \in \mathbb{R}^{n_{classes}}$ are trainable weights and biases. Then pass through the location classifier to predict spatial or positional labels:

$$\hat{l} = \text{soft max}(W_l M + b_l) \quad (10)$$

Where $W_l \in \mathbb{R}^{n_{locations} \times L}$ and $b_l \in \mathbb{R}^{n_{locations}}$.

The Multi-Instance Learning (MIL) module incorporates an Enhanced Gated Attention Network to aggregate instance-level features into sample-level representations. This design is particularly effective for binary and multi-class classification

tasks, where each sample consists of multiple instances, such as sequences. The core of the multi-instance learning module lies in its interpretable, trainable attention-pooling mechanism, which assigns learned attention scores to instances, enabling the model to focus on the most informative ones. This attention mechanism enhances the representation of critical features while suppressing noise, leading to more accurate and efficient classification. At the instance level, feature representations are generated using the attention scores, normalized via a softmax function, and aggregated into a sample-level representation. The final aggregated feature vector is then passed through a disease classifier for main task classification and a location classifier for spatial or positional predictions, ensuring a comprehensive and interpretable representation, as shown in Figure3b.

TABLE I. MAIN STAGES OF EAMIL ALGORITHM

| |
|---|
| Algorithm: Main process of EAMIL |
| Input: Dataset with N independent samples: $\{S_1, S_2, \dots, S_N\}$, where each sample S_i contains M sequences $\{S_i^1, S_i^2, \dots, S_i^M\}$. Each sample S_i corresponds to a label L_i . |
| Output: Predicted labels Y for test samples and Class probabilities. |
| Process: |
| <i>Initialization:</i> |
| Initialize model parameters and weights. |
| <i>Feature Extraction and Attention Computation:</i> |
| Input x : Feature matrix of size $N \times L$: |
| <i>Attention Computation:</i> |
| Compute Gate-based Attention: A_1 |
| Compute Spatial Sensitivity: A_2 . |
| Fuse Attention Scores: $A: A_1 + \lambda \times A_2$ |
| <i>Pseudo-labels:</i> |
| Use bag-level L_i of sample S_i to provide pseudo-labels. |
| <i>Loss Calculation:</i> |
| $L_{total} = c_1 \times L_{sample} + c_2 \times L_{instance}$. |
| Model training: Iteratively update model parameters. |
| Prediction: The learned model F predicts the label Y for test samples. |

- Training Strategy

1) *Instance-Level Supervision:* To bridge the gap between instance-level representations and sample-level labels, the model generates pseudo-labels for the top-k most informative instances based on their attention scores. These pseudo-labels are derived by combining true sample-level labels with the predicted attention distribution, as shown in Figure3d. For the top-k instances, the pseudo-labels are used to compute an instance-level loss:

$$L_p = \frac{1}{N_p} \sum_{i=1}^{N_p} L_{SVM}(\hat{y}_i, y_i) \quad (11)$$

where L_{SVM} denotes the smoothed top-1 SVM loss, \hat{y} represents the predicted label for instance i , y_i is the corresponding pseudo-label, and N_p is the number of pseudo-labeled instances.

2) *Sample-Level Supervision:* The primary classification loss compares the predicted sample-level labels \hat{y} with the ground-truth labels y using a cross-entropy loss:

$$L_s = L_{CE}(\hat{y}, y) \quad (12)$$

The total loss L_{total} is computed as a weighted combination of the sample-level and instance-level losses:

$$L_{total} = c_1 L_s + c_2 L_p \quad (13)$$

where $c_1 + c_2 = 1$ are hyperparameters controlling the balance between sample-level and instance-level supervision.

To align instance-level representations with sample-level labels, the model employs a pseudo-labeling approach for the top-k most informative instances, derived from their attention scores. These pseudo-labels are combined with sample-level ground truths to compute an instance-level loss using smoothed top-1 SVM loss. Simultaneously, sample-level supervision is applied by comparing the predicted sample-level labels with the ground-truth labels using a cross-entropy loss. The total loss is formulated as a weighted combination of the sample-level and instance-level losses, controlled by hyperparameters. This dual supervision strategy enables the model to effectively learn both instance-level and sample-level features, improving classification accuracy while maintaining interpretability and robustness.

III. RESULTS

EAMIL employs an integrated architecture that combines feature extraction, an enhanced gate attention module, and multi-instance deep learning modules to enable sophisticated analysis of complex immunogenomic data. This section first demonstrates the effectiveness of the EAMIL model in identifying SLE and RA through comparisons with transfer learning models and established deep learning approaches. Subsequently, we conduct an interpretability analysis based on the attention scores derived from the enhanced gate attention module. Specifically, we analyze the key genes and sequences identified by the model and validate these findings with supporting evidence. Furthermore, we perform a visualization analysis of the feature space. The model's performance is also evaluated on multi-classification tasks, including one-versus-other experiments and diagnostic analyses of affected sites in SLE patients, highlighting its potential applications in clinical scenarios. In addition, we investigate the model's performance on SLE samples stratified by SLEDAI scores, offering insights into disease-specific analyses. We also examine the impact of sample factors such as age and sex on the experimental results, providing comprehensive validation of EAMIL's performance. Using high-throughput sequencing data from 1,522 individuals (877 with SLE, 206 with RA, and 439 healthy controls), our experimental results demonstrate that EAMIL achieves state-of-the-art performance in both binary and multi-classification tasks. These findings establish EAMIL as a robust deep learning framework for the diagnostic analysis of autoimmune diseases..

A. Disease Prediction with Transfer-Learning Comparison

We first evaluated the ESMonehot encoding module in combination with several transfer learning models for SLE prediction. The multi-instance deep learning models adapted from pathology image detection included ABMIL, G-ABMIL, RRT, CLAM-SB, and CLAM-MB [22,23,24]. For each model, we replaced the original image coding module with our ESMonehot coding module, ported their architectures to autoimmune disease classification, and performed comparative experiments on the same dataset. Our EAMIL model combines a multi-instance deep learning framework after the ESMonehot module and enhanced gate attention to achieve SOTA performance on multiple metrics for binary classification tasks in both SLE and RA.

TABLE II. RESULTS OF THE SYSTEMIC LUPUS ERYTHEMATOSUS AND RHEUMATOID ARTHRITIS PREDICTION

| Disease | Methods | ACC | AUC | Pre | Recall | F1 |
|---------|--------------|--------------|--------------|--------------|--------------|--------------|
| SLE | ABMIL | 90.31 | 95.69 | 89.65 | 88.54 | 88.99 |
| | G-ABMIL | 93.44 | 97.93 | 92.89 | 92.36 | 92.60 |
| | RRT | 72.62 | 79.43 | 69.29 | 69.53 | 69.32 |
| | CLAM-SB | 90.47 | 95.78 | 89.87 | 88.65 | 89.15 |
| | CLAM-MB | 93.67 | 98.16 | 93.33 | 92.42 | 92.82 |
| | EAMIL | 95.12 | 98.95 | 94.59 | 94.47 | 94.51 |
| RA | ABMIL | 88.06 | 94.42 | 86.58 | 86.59 | 86.43 |
| | G-ABMIL | 90.23 | 95.98 | 89.38 | 87.93 | 88.57 |
| | RRT | 71.32 | 70.83 | 66.72 | 64.73 | 65.16 |
| | CLAM-SB | 89.77 | 95.53 | 88.65 | 88.11 | 88.25 |
| | CLAM-MB | 88.99 | 95.50 | 88.20 | 86.63 | 87.19 |
| | EAMIL | 92.71 | 97.76 | 91.62 | 91.70 | 91.62 |

The multibranching CLAM architecture (CLAM-MB) consistently outperformed the single-branching attention model (CLAM-SB) when using the same V gene and CDR3 sequence features, and our model outperformed both. This performance may reflect the subtle morphological differences between TCR rearrangements in patients with autoimmune diseases and those in healthy individuals, with the enhanced gate attention module and multi-branching facilitating the learning of different feature types. The results of SOTA on multiple metrics also fully validate the effectiveness of the PrimSeq strategy and the efficiency of ESMonehot encoding, highlighting the superior performance of EAMIL in autoimmune disease recognition. Our five-fold cross-validation shows that the model converges rapidly within 10 calendar hours and performs stably after approximately 20 calendar hours, further confirming the reliability of EAMIL in the SLE classification task.

We further validated our model on TCR repertoires from 206 RA patients and 439 healthy controls. Maintaining the same ESMonehot encoding method and V gene and CDR3 feature selection, we compared EAMIL with other transfer learning models for RA prediction. The results demonstrate EAMIL's consistent performance across autoimmune conditions, with excellent metrics across all evaluation criteria, confirming the model's adaptability. Additionally, the G-ABMIL model with ESMonehot encoding achieved impressive performance, further validating our encoding methodology's effectiveness and highlighting EAMIL's stability and reliability in diverse autoimmune disease prediction contexts.

B. Comparison with Existing Methods

We conducted comprehensive comparisons between EAMIL and current repertoire classification algorithms, specifically DeepTCR and DeepTAPE, using datasets from SLE and RA patients and healthy individuals [16,18]. DeepTCR models complex TCR sequences by learning from labeled data for repertoire classification, while DeepTAPE combines CNN and LSTM modules for unified repertoire classification. Maintaining consistent learning parameters and utilizing identical V gene and CDR3 sequence features as input, we performed binary classification tasks for both SLE and RA versus healthy controls.

Implementing five-fold cross-validation with 50 training sequences per iteration, we systematically compared the AUC metrics of DeepTCR, DeepTAPE, and EAMIL, as shown in Figure4. Our results demonstrate that EAMIL consistently

outperforms both comparison algorithms across both disease classification scenarios. These findings validate EAMIL's effectiveness for TCR sequence classification and highlight its potential for analyzing complex immunogenomic data.

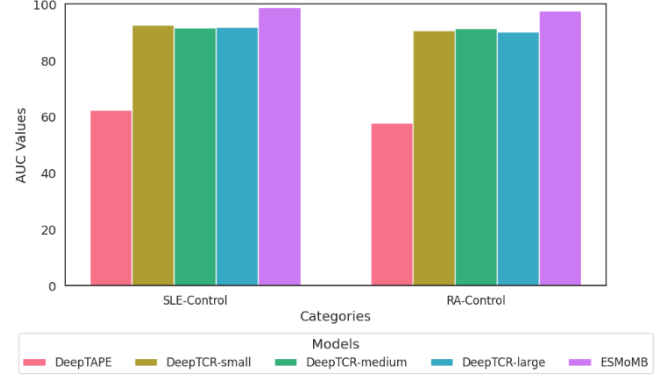


Fig. 4. Comparison of Results with existing deep learning methods. We conducted comparative experiments between our model and DeepTCR and DeepTAPE using the two disease cases on the AUC metric, where DeepTCR contains small, medium and large settings.

C. Significant Genes and Sequences Identification

To demonstrate EAMIL's capability to recognize immunologically significant features, we analyzed attention heatmaps from randomly selected samples in both disease categories. For SLE patients, we aggregated attention scores across all samples and identified the top 10 sequences with highest attention values, as shown in Figure5a. Notably, these sequences aligned precisely with significantly differential sequences previously identified in independent analyses[11]. The model successfully recognized SLE-specific gene families, particularly TRBV13 and TRBV5, which are exclusively observed in SLE patients, validating EAMIL's ability to identify disease-associated molecular features. Similarly, in RA patient samples, attention score aggregation revealed that 28 of the top 30 highest-scoring sequences corresponded with previously reported RA-associated sequences, as shown in Figure5b. This remarkable concordance demonstrates EAMIL's robust capability to identify disease-relevant genetic elements, providing valuable insights for disease analysis and potential therapeutic development. To visualize feature distribution after attention processing, we generated t-SNE plots for both SLE-Control and RA-Control comparisons, as shown in Figure5c and Figure5d. The resulting visualizations show nearly complete separation between disease states, underscoring the effectiveness of our PrimeSeq strategy, ESMonehot module, and enhanced gate attention module in feature learning and discrimination.

The genes identified by the model as potentially associated with the pathogenesis of systemic lupus erythematosus (SLE) and rheumatoid arthritis (RA) were validated through an extensive literature review. The vast majority of the top-ranked genes were found to be directly or indirectly implicated in disease pathogenesis. Notably, the TRBV2801* gene exhibited a down-regulated effect in both SLE and RA, while the TRBV2701* gene demonstrated an indirect up-regulation effect in both diseases. Studies have further shown that the TRBV6-101* gene is significantly enriched in SLE patients, whereas TRBV6-201* is markedly down-regulated. The TRBV202* gene has been positively correlated with the SLE

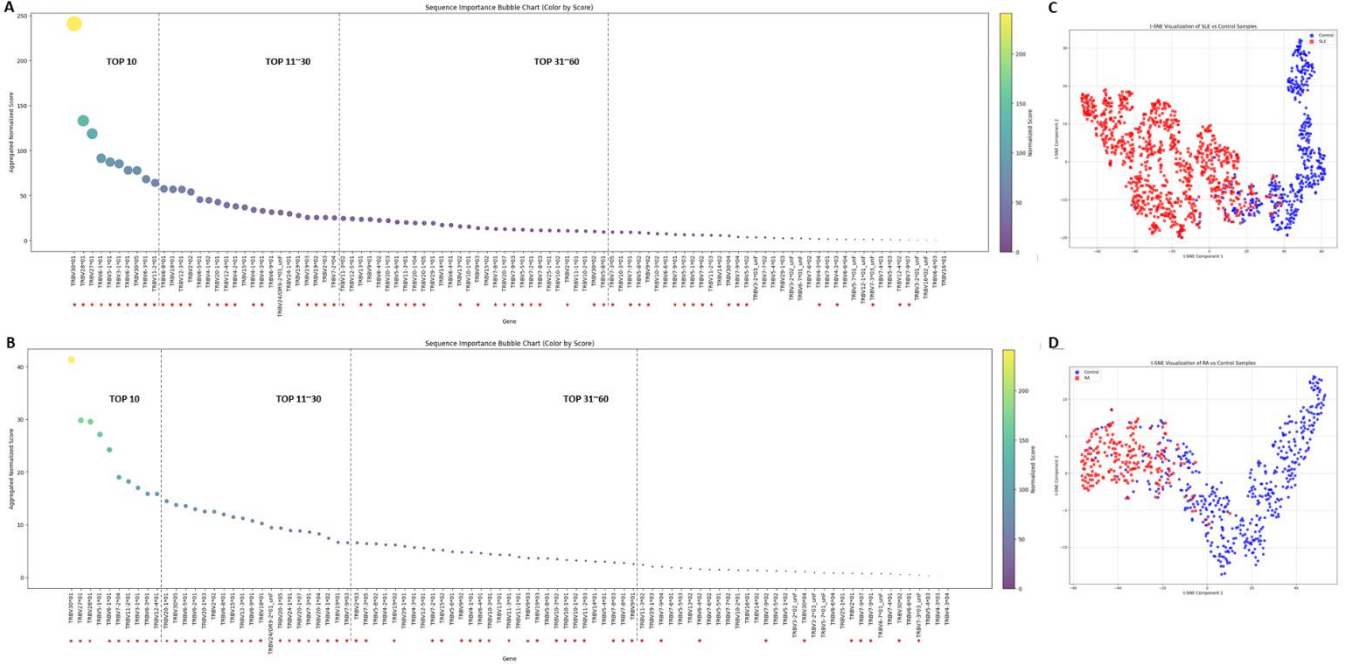


Fig. 5. Visual analysis of significant genes and features. To identify significant genes in SLE and rheumatoid arthritis patients, we counted the top 10 sequences cumulatively identified by our model for all SLE and rheumatoid arthritis patients and plotted them as bubble plots, where a bubble corresponds to a gene, with higher scores denoting more significant genes. We labeled the genes in SLE and rheumatoid arthritis patients that matched previous studies with red stars (A,B). We plotted T-SNE plots for SLE controls and RA controls to show the distribution of SLE-encoded post-VCDR3 features (C) and RA-encoded post-VCDR3 features (D).

TABLE III. GENE VALIDATION OF THE SYSTEMIC LUPUS ERYTHEMATOSUS AND RHEUMATOID ARTHRITIS PREDICTION

| Disease | Genes | Relationship | Validation |
|---------|-------------|----------------|----------------|
| SLE | TRBV28*01 | downregulation | Direct [26] |
| | TRBV27*01 | upregulation | Indirect [27] |
| | TRBV6-1*01 | other activity | Direct [28] |
| | TRBV5-1*01 | downregulation | Direct [26] |
| | TRBV3-1*01 | downregulation | Direct [26] |
| | TRBV6-2*01 | downregulation | Direct [26,28] |
| | TRBV6-3*01 | downregulation | Direct [26] |
| | TRBV11-2*01 | other activity | Direct [26] |
| | TRBV6-8*01 | upregulation | Indirect [29] |
| | TRBV18*01 | other activity | Indirect [29] |
| RA | TRBV2*02 | other activity | Direct [30] |
| | TRBV27*01 | upregulation | Indirect [27] |
| | TRBV28*01 | downregulation | Direct [11] |
| | TABV5-1*01 | other activity | Direct [31] |
| | TRBV6-1*01 | other activity | Direct [11] |
| | TRBV7-2*04 | upregulation | Direct [27] |
| | TRBV11-2*01 | other activity | Indirect [32] |
| | TRBV6-3*01 | other activity | Indirect [33] |
| | TRBV12-4*01 | upregulation | Direct [29] |
| | TRBV20-1*01 | upregulation | Direct [29] |
| | TRBV6-2*01 | other activity | Direct [11] |
| | TRBV2*02 | other activity | Direct [30] |

Disease Activity Index (SLEDAI). In RA, the TABV5-101* gene is highly expressed in T cells infiltrating synovial tissues, and TRBV11-201* is associated with Th17-mediated inflammation. Additionally, TRBV202* has demonstrated a significant correlation with RA disease activity, as measured by the Disease Activity Score (DAS28), as shown in tabel3. The strong alignment of these findings with prior studies

underscores the efficacy of the feature extraction and enhanced attention module employed by EAMIL. This robust model performance provides a powerful framework for identifying potential disease-associated genes, offering profound implications for clinical diagnosis and analysis.

D. Multiclassification Comparative Experiments

To evaluate the multiclassification capabilities of EAMIL, we constructed a three-class prediction task using TCR rearrangement data from all 1522 individuals (SLE, arthritis, and healthy controls). EAMIL performed well on this complex task, with an AUC 3.4% higher than G-ABMIL and an accuracy of 6.99% higher than G-ABMIL. EAMIL's F1 score greatly exceeds that of all other transfer learning models, confirming its great strength in multi-class discrimination, as shown in tabel4. These results validate the excellent performance of EAMIL in multi-category classification, which is important for clinical disease diagnosis and differential analysis.

TABLE IV. RESULTS OF MULTICLASSIFICATION

| Methods | ACC | AUC | Pre | Recall | F1 |
|--------------|--------------|--------------|--------------|--------------|--------------|
| ABMIL | 80.23 | 92.01 | 72.04 | 63.21 | 61.97 |
| G-ABMIL | 80.29 | 92.66 | 70.36 | 65.45 | 63.49 |
| RRT | 64.86 | 72.50 | 45.68 | 48.87 | 46.69 |
| CLAM-SB | 81.54 | 93.08 | 72.1 | 65.00 | 64.14 |
| CLAM-MB | 81.41 | 93.20 | 71.06 | 66.79 | 67.02 |
| EAMIL | 87.28 | 96.06 | 82.27 | 79.28 | 80.39 |

E. One Versus Others Experiments

To evaluate EAMIL's ability to recognize specific disease states within a heterogeneous population—a critical capability for clinical diagnosis—we conducted a comprehensive “one-on-one” experiment across a dataset comprising 1,522

individuals. The analysis focused on identifying patients with systemic lupus erythematosus (SLE) and rheumatoid arthritis (RA) as distinct subgroups. EAMIL demonstrated robust performance in SLE identification, achieving an area under the curve (AUC) of 94.53% and an accuracy (ACC) of 86.08%, as shown in Figure6a. In contrast, the model's relatively lower detection performance for RA may be attributed to category imbalance, driven by the smaller sample size of RA cases compared to other categories, as well as potential feature overlap with other diseases exhibiting similar characteristics. Notably, when tasked with distinguishing SLE from RA, EAMIL achieved an AUC of 84.66% and an ACC of 83.95%, providing a valuable reference point for clinical diagnostic analysis. Moreover, EAMIL demonstrated exceptional performance in differentiating healthy individuals from patients with autoimmune diseases, with an AUC of 96.28% and an ACC of 90.51%. These results underscore the model's strong potential for accurate diagnosis of autoimmune diseases, highlighting its utility in clinical applications.

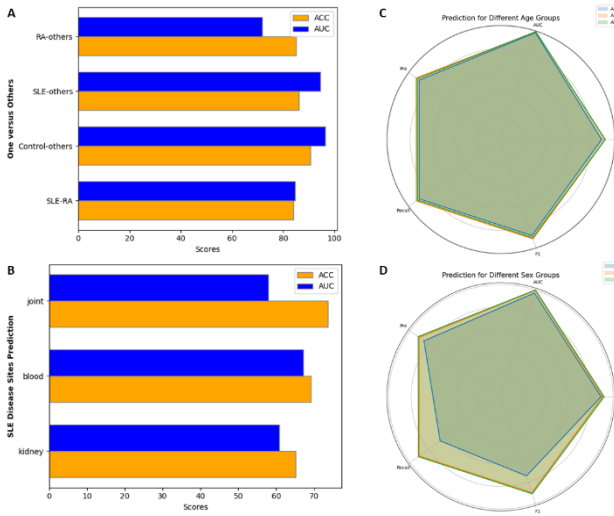


Fig. 6. Results of Analysis Experiments. (A) One-vs-Others Experiments Results. The outcomes of one-vs-others experiments are plotted for each of the three states: SLE, RA, and Control. (B) Identification of Damaged Body Parts in SLE Patients. Diagnostic analysis was performed to identify damaged sites in SLE patients labeled with affected areas. (C, D) Analysis of SLE Patients with Different Characteristics. (C) Gender-based analysis of SLE patients. (D) Age group-based analysis of SLE patients. Radar charts present the five-fold cross-validation results, adjusted by subtracting 50%.

F. SLE Organ-specific Damage Identification

Based on the exceptional performance of our model in disease diagnosis, we further explored its potential in identifying organ damage in patients with systemic lupus erythematosus (SLE). Specifically, we focused on classifying damage versus non-damage in the blood, kidney, and joint systems using clinical data from SLE patients. Similar to previous experiments, we employed a five-fold cross-validation approach. Notably, we incorporated C3 and C4 levels from the clinical data—key components of the complement system and critical markers of immune function. These proteins, the third and fourth components of the complement cascade, are widely used in the evaluation of immune system activity, particularly in studies and diagnostics related to autoimmune diseases [34,35]. By integrating sample information with feature data, we

conducted a five-fold cross-validation experiment across all labeled SLE patients. On the blood damage classification task, our model achieved an AUC of 67.18%, significantly outperforming DeepTCR, which achieved an AUC of 55.97%. This represents a noteworthy advancement in the identification of organ-specific damage, as illustrated in Figure6b. These preliminary results highlight the potential of our approach to provide valuable insights for the clinical diagnosis of SLE-related organ damage.

G. SLEDAI Comparative Experiment

The Systemic Lupus Erythematosus Disease Activity Index (SLEDAI) is a validated clinical tool for assessing SLE disease activity, guiding treatment decisions including corticosteroid dosing and immunosuppressant selection, while facilitating disease monitoring and management. SLEDAI scores of 0-4 typically indicate quiescent disease, while scores >4 signify active disease, with higher scores reflecting increased severity [25]. We analyzed TCR repertoire data from 873 SLE patients with documented SLEDAI scores (312 quiescent, 561 active) and 439 healthy controls.

EAMIL demonstrated significantly greater discriminatory power in distinguishing active SLE from controls compared to differentiating quiescent SLE from controls, achieving an F1 score of 94.61% for active disease (2.36% higher than for quiescent disease). This finding aligns with clinical observations that active SLE presents more distinct immunological profiles, facilitating model recognition. Notably, even for the more challenging task of discriminating quiescent SLE from controls, EAMIL maintained robust performance with AUC and accuracy of 98.26% and 92.52%, respectively. These results confirm EAMIL's effectiveness for autoimmune disease detection across disease activity states and suggest potential applications for early diagnosis and precision treatment approaches. Comparing EAMIL's performance in distinguishing all SLE patients from controls revealed slight superiority in AUC and F1 metrics for active disease discrimination, without significant advantages in accuracy, as shown in Figure7. This suggests that while active disease contributes substantially to model training, the more challenging quiescent SLE discrimination remains valuable for overall SLE detection.

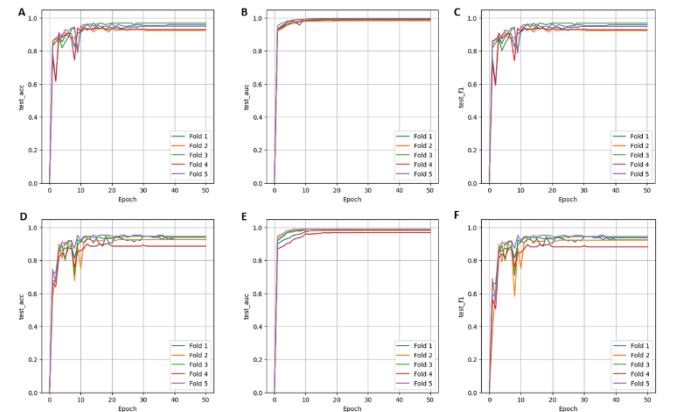


Fig. 7. Results of SLEDAI Experiments. We used all SLE patients containing both Active and Slient states, the first line for the identification of Active SLE patients(A-C) and the second line for the identification of Active SLE patients(D-F).

H. Limited Impact of Age and Sex on SLE Disease Identification

Having established EAMIL's efficacy for SLE classification, we investigated potential confounding effects of demographic factors. We stratified 873 SLE patients by age using the median (35 years) as threshold and compared classification performance against 439 healthy controls. Results revealed superior performance across all metrics for patients >35 years compared to those \leq 35 years, indicating age-related effects on classification. This aligns with known immunological changes during aging, as shown in Figure6c, including altered immune cell function, cytokine secretion, and gene expression regulation. Elderly patients typically exhibit characteristics of immune aging characterized by increased chronic inflammation and enhanced autoimmune responses, potentially manifesting more pronounced disease signatures that facilitate model classification.

Regarding sex differences, we compared classification performance between male SLE patients (n=99) versus controls and female SLE patients (n=774) versus controls. Female cohort classification consistently outperformed male cohort classification across all metrics, suggesting sex-based influences on model performance, as shown in Figure6d. This corresponds with SLE's established sex bias, with substantially higher prevalence in females, potentially related to estrogen's immunomodulatory effects that may enhance immune responses and exacerbate autoimmune manifestations. Additionally, the smaller male sample size likely contributed to reduced classification performance relative to the female cohort.

Overall, while older patients and female patients demonstrated more readily recognizable disease characteristics, the differences in accuracy and AUC between age and sex strata remained modest, confirming that EAMIL effectively learns disease-specific features with limited influence from demographic factors on overall model performance.

IV. DISCUSSION

In this study, we have successfully developed and validated EAMIL, a multimodal multi-instance deep learning model based on the PrimeSeq sequence extraction strategy for TCR sequence analysis and autoimmune disease identification. Our ESMonehot encoding effectively integrates diverse information sources including gene segments and amino acid sequences, while the multi-instance module's enhanced attention mechanism provides interpretability through identification of disease-relevant features, establishing the foundation for instance clustering and pseudo-label generation. EAMIL accomplishes autoimmune disease classification by efficiently analyzing extensive TCR sequence data and identifying key sequences through quantitative attention scores.

Experimental evaluation demonstrates EAMIL's exceptional performance in identifying both SLE and RA, with robust results in multiclass discrimination tasks. For SLE prediction specifically, the model achieved SOTA metrics across AUC and accuracy, with particularly noteworthy performance in distinguishing between SLE patients stratified by SLEDAI scores and healthy controls. EAMIL has shown potential in diagnosing organ damage in SLE patients and has maintained strong performance even when faced with potential confounding factors such as age and sex. Importantly, the model successfully learned disease-relevant and genes,

enabling accurate recognition and differentiation between distinct autoimmune conditions—findings with significant implications for clinical diagnosis and therapeutic development.

Future research will focus on incorporating additional autoimmune disease datasets to further enhance EAMIL performance and generalizability. Expanding applications to other autoimmune conditions and integrating clinical data for more comprehensive disease characterization represent promising research directions. We anticipate that cross-disciplinary approaches will facilitate improved identification of disease-associated receptors, opening new avenues for diagnostic analysis and therapeutic development in autoimmune diseases.

As deep learning technologies continue to advance and biomedical data resources expand, we anticipate that EAMIL will make increasingly significant contributions to precision medicine approaches for autoimmune diseases. Through ongoing algorithm optimization and model refinement, EAMIL has substantial potential to become an important diagnostic tool in autoimmune disease prediction and classification.

REFERENCES

- [1] Chi, Xinxin, et al. "Innate and adaptive immune abnormalities underlying autoimmune diseases: the genetic connections." *Science China Life Sciences* 66.7 (2023): 1482-1517.
- [2] Bach, Jean-François. "The hygiene hypothesis in autoimmunity: the role of pathogens and commensals." *Nature Reviews Immunology* 18.2 (2018): 105-120.
- [3] Koch-Henriksen, Nils, and Per Soelberg Sørensen. "The changing demographic pattern of multiple sclerosis epidemiology." *The Lancet Neurology* 9.5 (2010): 520-532.
- [4] Fanouriakis, Antonis, et al. "Update on the diagnosis and management of systemic lupus erythematosus." *Annals of the rheumatic diseases* 80.1 (2021): 14-25.
- [5] Ameer, Muhammad Atif, et al. "An overview of systemic lupus erythematosus (SLE) pathogenesis, classification, and management." *Cureus* 14.10 (2022).
- [6] Kondo, Naoki, Takeshi Kuroda, and Daisuke Kobayashi. "Cytokine networks in the pathogenesis of rheumatoid arthritis." *International journal of molecular sciences* 22.20 (2021): 10922.
- [7] Frazzei, Giulia, et al. "Preclinical autoimmune disease: a comparison of rheumatoid arthritis, systemic lupus erythematosus, multiple sclerosis and type 1 diabetes." *Frontiers in immunology* 13 (2022): 899372.
- [8] Milo, Ron, and Ariel Miller. "Revised diagnostic criteria of multiple sclerosis." *Autoimmunity reviews* 13.4-5 (2014): 518-524.
- [9] Kavanaugh, Arthur, et al. "Guidelines for clinical use of the antinuclear antibody test and tests for specific autoantibodies to nuclear antigens." *Archives of pathology & laboratory medicine* 124.1 (2000): 71-81.
- [10] Sui, Weiguo, et al. "Composition and variation analysis of the TCR β -chain CDR3 repertoire in systemic lupus erythematosus using high-throughput sequencing." *Molecular immunology* 67.2 (2015): 455-464.
- [11] Liu, Xiao, et al. "T cell receptor β repertoires as novel diagnostic markers for systemic lupus erythematosus and rheumatoid arthritis." *Annals of the rheumatic diseases* 78.8 (2019): 1070-1078.
- [12] Hwang, Jeong-Ryul, et al. "Recent insights of T cell receptor-mediated signaling pathways for T cell activation and development." *Experimental & molecular medicine* 52.5 (2020): 750-761.
- [13] Shah, Kinjal, et al. "T cell receptor (TCR) signaling in health and disease." *Signal transduction and targeted therapy* 6.1 (2021): 412.
- [14] Schepers, Wouter, et al. "Low and variable tumor reactivity of the intratumoral TCR repertoire in human cancers." *Nature medicine* 25.1 (2019): 89-94.

- [15] Pavlović, Milena, et al. "The immuneML ecosystem for machine learning analysis of adaptive immune receptor repertoires." *Nature Machine Intelligence* 3.11 (2021): 936-944.
- [16] Sidhom, John-William, et al. "DeepTCR is a deep learning framework for revealing sequence concepts within T-cell repertoires." *Nature communications* 12.1 (2021): 1605.
- [17] Zaslavsky, Maxim E., et al. "Disease diagnostics using machine learning of B cell and T cell receptor sequences." *Science* 387.6736 (2025): eadp2407.
- [18] Shen, Tongfei, et al. "DeepTAPE: Enhancing Systemic Lupus Erythematosus Diagnosis with Deep Learning Based on TCR β CDR3 Sequences." 2024 IEEE International Conference on Bioinformatics and Biomedicine (BIBM). IEEE, 2024.
- [19] Sarumi, Oluwafemi A., and Dominik Heider. "Large language models and their applications in bioinformatics." *Computational and Structural Biotechnology Journal* (2024).
- [20] Lin, Zeming, et al. "Evolutionary-scale prediction of atomic-level protein structure with a language model." *Science* 379.6637 (2023): 1123-1130.
- [21] Wang, Xinggang, et al. "Revisiting multiple instance neural networks." *Pattern recognition* 74 (2018): 15-24.
- [22] Ilse, Maximilian, Jakub Tomczak, and Max Welling. "Attention-based deep multiple instance learning." *International conference on machine learning*. PMLR, 2018.
- [23] Lu, Ming Y., et al. "Data-efficient and weakly supervised computational pathology on whole-slide images." *Nature biomedical engineering* 5.6 (2021): 555-570.
- [24] Tang, Wenhao, et al. "Feature re-embedding: Towards foundation model-level performance in computational pathology." *Proceedings of the IEEE/CVF Conference on Computer Vision and Pattern Recognition*. 2024.
- [25] Guthridge, Joel M., et al. "Adults with systemic lupus exhibit distinct molecular phenotypes in a cross-sectional study." *EClinicalMedicine* 20 (2020).
- [26] Zeng, Li, et al. "Unravelling the TCR β repertoire: a key to unlocking the immunopathogenesis and precision medicine in SLE." *Lupus Science & Medicine* 12.1 (2025).
- [27] Ye, Xiaolan, et al. "High-throughput sequencing-based analysis of T cell repertoire in lupus nephritis." *Frontiers in immunology* 11 (2020): 1618.
- [28] Sui, Weiguo, et al. "Composition and variation analysis of the TCR β -chain CDR3 repertoire in systemic lupus erythematosus using high-throughput sequencing." *Molecular immunology* 67.2 (2015): 455-464.
- [29] Liu, Qi, et al. "Bulk T-cell receptor sequencing confirms clonality in obstetric antiphospholipid syndrome and may as a potential biomarker." *Autoimmunity* 57.1 (2024): 2360490.
- [30] Zhang, Qin, et al. "Integrated analysis of lncRNA, miRNA and mRNA expression profiling in patients with systemic lupus erythematosus." *Archives of Medical Science* 15.4 (2019): 872-879.
- [31] Klarenbeek, P. L., et al. "Inflamed target tissue provides a specific niche for highly expanded T-cell clones in early human autoimmune disease." *Annals of the rheumatic diseases* 71.6 (2012): 1088-1093.
- [32] Jakiela, B., et al. "Facilitated expansion of Th17 cells in lupus nephritis patients." *Clinical & Experimental Immunology* 194.3 (2018): 283-294.
- [33] Yu, Aixin, et al. "The lower limit of regulatory CD4 $^{+}$ Foxp3 $^{+}$ TCR β repertoire diversity required to control autoimmunity." *The Journal of Immunology* 198.8 (2017): 3127-3135.
- [34] Ricklin, Daniel, et al. "Complement: a key system for immune surveillance and homeostasis." *Nature immunology* 11.9 (2010): 785-797.
- [35] Olfieriev, Mikhail, et al. "Measuring interferon alpha and other cytokines in SLE." *Systemic Lupus Erythematosus: Methods and Protocols* (2014): 131-150.